THE JOURNAL OF BIOLOGICAL CHEMISTRY VOL. 282, NO. 13, pp. 9646–9656, March 30, 2007

Tautomerism of Histidine 64 Associated with Proton Transfer in Catalysis of Carbonic Anhydrase*

Received for publication, October 13, 2006, and in revised form, January 2, 2007 Published, JBC Papers in Press, January 3, 2007, DOI 10.1074/jbc.M609679200

Hideto Shimahara[‡§¶], Takuya Yoshida[§], Yasutaka Shibata[§], Masato Shimizu[¶], Yoshimasa Kyogoku[¶], Fumio Sakiyama[¶], Takashi Nakazawa[‖], Shin-ichi Tate[‡], Shin-ya Ohki[‡], Takeshi Kato[‡‡], Hozumi Moriyama[‡‡], Ken-ichi Kishida[‡‡], Yasuo Tano[‡‡], Tadayasu Ohkubo[§], and Yuji Kobayashi[§**1]**

*From the [‡]Center for Nano Materials and Technology, Japan Advanced Institute of Science and Technology, Nomi, Ishikawa 923-1211, the [¶]Institute for Protein Research, Osaka University, Suita, Osaka 565-0871, the [‖]Department of Chemistry, Nara Women's University, Nara 630-8506, the [‡‡]Medical School Osaka University, Suita, Osaka 565-0871, the [§]Graduate School of Pharmaceutical Sciences, Osaka University, Suita, Osaka 565-0871, and the **Osaka University of Pharmaceutical Sciences, Takatsuki, Osaka 569-1094, Japan*

The imidazole ^{15}N signals of histidine 64 (His^{64}), involved in the catalytic function of human carbonic anhydrase II (hCAII), were assigned unambiguously. This was accomplished by incorporating the labeled histidine as probes for solution NMR analysis, with ^{15}N at *ring*-N$^{\delta1}$ and N$^{\epsilon2}$, ^{13}C at *ring*-Cϵ1, ^{13}C and ^{15}N at all carbon and nitrogen, or ^{15}N at the amide nitrogen and the labeled glycine with ^{13}C at the carbonyl carbon. Using the pH dependence of *ring*-^{15}N signals and a comparison between experimental and simulated curves, we determined that the tautomeric equilibrium constant (K_T) of His^{64} is 1.0, which differs from that of other histidine residues. This unique value characterizes the imidazole nitrogen atoms of His^{64} as both a general acid (*a*) and base (*b*): its ϵ2-nitrogen as (*a*) releases one proton into the bulk, whereas its δ1-nitrogen as (*b*) extracts another proton from a water molecule within the water bridge coupling to the zinc-bound water inside the cave. This accelerates the generation of zinc-bound hydroxide to react with the carbon dioxide. Releasing the productive bicarbonate ion from the inside separates the water bridge pathway, in which the next water molecules move into beside zinc ion. A new water molecule is supplied from the bulk to near the δ1-nitrogen of His^{64}. These reconstitute the water bridge. Based on these features, we suggest here a catalytic mechanism for hCAII: the tautomerization of His^{64} can mediate the transfers of both protons and water molecules at a neutral pH with high efficiency, requiring no time- or energy-consuming processes.

Carbonic anhydrase (CA)[2] (EC 4.2.1.1) is a ubiquitous enzyme that catalyzes the reversible hydration of carbon dioxide (1). Isozymes of carbonic anhydrase regulate or function in such diverse physiological processes as pH regulation, ion transport, water-electrolyte balance, bicarbonate secretion-absorption, bone resorption, maintenance of intraocular pressure, renal acidification, and brain development (2). Nonfunctioning CA is implicated in such diseases as osteopetrosis syndrome, glaucoma, respiratory acidosis, epilepsy, and Ménière syndrome. Diseases due to CA deficiency include those affecting bones, the brain, and the kidneys. Consequently determining the detailed structure/function relationships or mechanisms responsible for its catalytic properties is mandatory for developing inhibitors or replacement therapies.

CA is present in at least three gene families (α, β, and γ), which has made it a popular model for the study of the evolution of gene families and protein folding, and for transgenic and gene target studies (2). Among the three families, the α family is the best characterized, with 11 known isozymes identified in mammals. Earnhardt and co-workers have summarized maximal k_{cat} and k_{cat}/K_m values for CO_2 hydration by isozyme I–VII (3). The human isozyme II (hCAII) has a remarkably high turnover rate or catalytic efficiency ($k_{cat}/K_m = 1.5 \times 10^8\ M^{-1}\ s^{-1}$) that is very close to the frequency with which the enzyme and substrate molecules collide with each other in solution.

It is widely accepted that the hydration of CO_2 catalyzed by hCAII proceeds through several chemical steps as shown in Scheme 1 (1, 4, 5): the direct nucleophilic attack of the zinc-bound hydroxide ion on the carbonyl carbon of substrate CO_2 (structures 1–2), the formation of a zinc-bound bicarbonate intermediate (structures 2–3), the isomerization of the bicarbonate ion (structures 3–4), the exchange of the product bicarbonate ion with a H_2O (structures 4–5), and the regeneration of the zinc-bound hydroxide ion by the transfer of a proton to bulk solvent (structures 1–5). The proton transfer step (structures 1–5) consists of two substeps: 1) an intra-molecular transfer of protons to another residue in the enzyme and 2) a release of protons to the outside of the enzyme with the aid of a base. The intra-molecular proton transfer is the rate-limiting step of the maximal turnover rate ($10^6\ s^{-1}$) at high concentrations of a base, whereas the proton release into the medium is rate-limiting at low buffer concentrations.

* This work was supported by Japan Foundation for Applied Enzymology, Grants-in-aid for Scientific Research 09307054 and 13780482 from the Ministry of Education, Science, Sports and Culture of Japan, and a Grant for Promotion of JAIST Research Projects. The costs of publication of this article were defrayed in part by the payment of page charges. This article must therefore be hereby marked "*advertisement*" in accordance with 18 U.S.C. Section 1734 solely to indicate this fact.

[1] To whom correspondence should be addressed. Tel.: 81-72-690-1080; Fax: 81-72-690-1080; E-mail: kobayasi@gly.oups.ac.jp.

[2] The abbreviations used are: CA, carbonic anhydrase; hCAII, human carbonic anhydrase II; [*ring*-^{15}N]His, histidine labeled with ^{15}N at the *ring*-N$^{\delta1}$ and N$^{\epsilon2}$; [U-^{13}C/^{15}N]His, histidine labeled with ^{13}C and ^{15}N at all carbon and nitrogen nuclei; [*ring*-C$^{\epsilon1}$-^{13}C]His, histidine labeled with ^{13}C at the *ring*-C$^{\epsilon1}$; HSQC, heteronuclear single quantum coherence spectroscopy; HNCO, ^{1}H-^{15}N-^{13}C correlation spectroscopy via $J_{N\text{-}H}$ and $J_{N\text{-}CO}$; HNCA, ^{1}H-^{15}N-^{13}C correlation spectroscopy via $J_{N\text{-}H}$ and $J_{N\text{-}C\alpha}$; HCCH, ^{1}H-^{13}C-^{13}C-^{1}H correlation spectroscopy via $J_{C\alpha\text{-}H}$, $J_{C\text{-}C}$, and $J_{C\beta\text{-}H}$; (Hβ)Cβ(CγCδ)Hδ, ^{1}H-^{13}C-^{13}C-^{13}C-^{1}H correlation spectroscopy via $J_{C\beta\text{-}H}$, $J_{C\text{-}C}$ and $J_{C\delta\text{-}H}$; imidazole H_N, H$^{\delta1}$ or H$^{\epsilon2}$ of histidine; >N-H, pyrrole-like nitrogen; >N:, pyridine-like nitrogen; +>N-H, positively charged nitrogen.

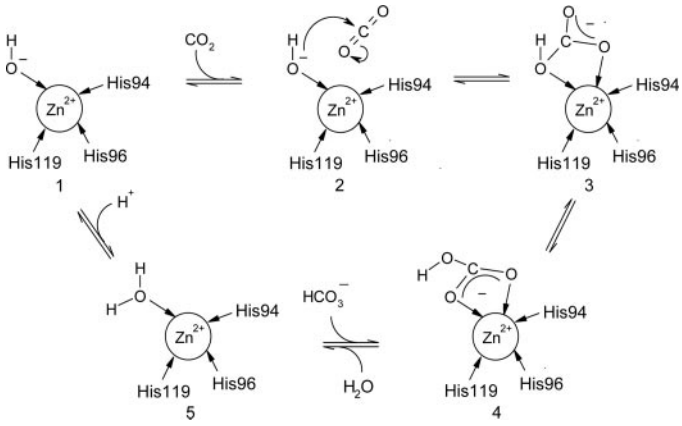

SCHEME 1

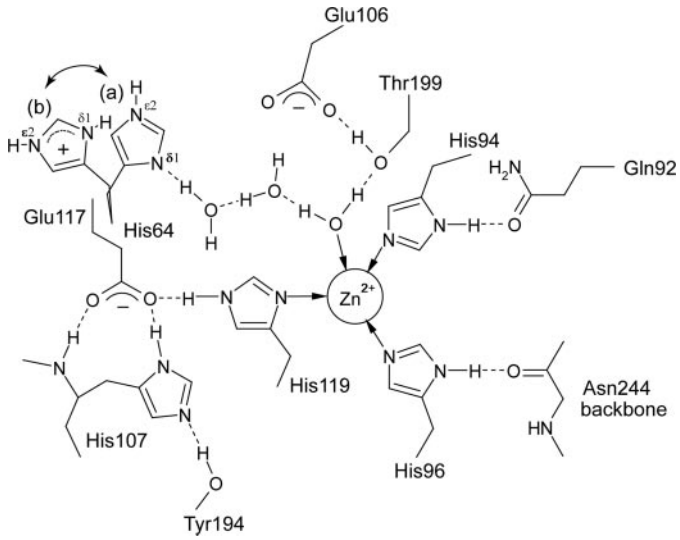

FIGURE 1. **The active site of the hCAII.** The efficient catalysis of hCAII requires the zinc ion to be tetrahedrally coordinated to three imidazole groups of His^{94}, His^{96}, and His^{119}, which are located at a bottom of the conical cleft about 15 Å wide and 15 Å deep. The fourth ligand to the zinc ion is a solvent molecule. These four ligands are packed in a large hydrogen bond network: His^{94}–Gln^{92}, His^{96}–Asn^{244}, His^{119}–Glu^{117}–His^{107}–Tyr^{194}, and the zinc-bound solvent molecule, Thr^{199}–Glu^{106}. His^{64} is located through the water bridge about 7.5 Å away from the zinc ion on the wall of the active site cleft. A swinging movement is found in the equilibrium between structures *a* and *b*.

In this reaction mechanism, His^{64} is thought to play an important role in shuttling protons between the inside and outside of the active site cleft (6–9). As depicted in Fig. 1, the "in" (**a**) and "out" (**b**) conformations, representing the direction of the imidazole ring toward and away from the active site, were observed in pH-dependent x-ray crystallographic studies of hCAII (4, 5, 10–12). The side chain imidazole ring takes the in conformation at pH 7.8, where His^{64} should be electrically neutral because of the pK_a value of 7 as determined by ^1H NMR (13). In this conformation, the δ1-nitrogen of His^{64} appears to be involved in a water bridge or solvent network connected to the zinc-bound hydroxide ion through a hydrogen bond (12, 14, 15). In contrast, the T200S mutant of this enzyme was found to have His^{64} in the out conformation at pH 8.0, retaining the full enzymatic activity (16). Because the out conformation of the imidazole ring was also observed at pH 5.7 (10), a swinging movement between the in and out conformations was assumed in connection with the proton transfer between a water molecule near a zinc ion and a bulk water molecule (5): the productive proton, which is transferred to the δ1-nitrogen via the water bridge, is released from its nitrogen to the bulk solution after swinging of the imidazole ring. This model is attractive because it appears to be able to account for a flow of water molecules in terms of space shared with the imidazole ring. However, there is no evidence supporting the notion that the two conformers are in the kinetically stable state at a given pH. In addition, molecular dynamics simulations show that His^{64} vibrates rather than swings; it could be flexible enough to find the optimum geometry between active site solvent molecules and the bulk solvent (17–19).

Despite much effort, the proton-transfer mechanism involving the dynamic behavior of His^{64} still remains controversial: the specific or reasonable manner in which His^{64} participates in the proton-transfer needs to be explored. To address these issues, we labeled His^{64} with ^{15}N nucleus to identify the tautomeric forms of the imidazole ring in connection with the chemical mechanism of proton transfer in hCAII. The goal of our study is to detail the mechanisms responsible for the catalytic properties of carbonic anhydrase.

MATERIALS AND METHODS

Isotope Labeling of hCAII—To detect imidazole ^{15}N signals and assign one of them to His^{64}, selectively labeled enzymes were obtained from a double-auxotroph requiring glycine and histidine of bacterial cell *Eschericha coli* BL21(DE3) containing the pET-hCAII gene and pLys-S, grown in the presence of labeled histidines and/or glycine. The double auxotroph was prepared using two distinct procedures. First is the generalized transduction method using phage P1 *vir* (20). In this experiment, the *glyA* gene encoding the serine-glycine hydroxymethyl transferase in the chromosome of *E. coli* BL21(DE3) (21) was replaced with the deficient gene *glyA*6 in the chromosome of a glycine auxotroph *E. coli* IQ417 (22) via the P1 phage particle. The second procedure is the ampicillin treatment method for the isolation of histidine auxotrophic mutants (23). The cells treated with 0–4 μg/ml acridine mutagen ICR191 (6-chloro-9-[3-(2-chloroethylamino)-propylamino]-2-methoxy-acridine dihydrochloride, Sigma) were grown in an M9 medium containing 50 μg/ml ampicillin to enrich histidine auxotroph. The isolated double auxotroph requiring histidine and glycine, designated HS004, was cultured in an M9 medium containing 20 μg/ml histidine and 80 μg/ml glycine at 37 °C. By using this auxotroph transformed by the pET-hCAII-gene plasmid, four types of selectively labeled enzymes ([*ring*-^{15}N]His-hCAII, [*ring*-$C^{\epsilon 1}$-^{13}C]His-hCAII, [U-^{13}C/^{15}N]His-hCAII, and [α-^{15}N]His/[1-^{13}C]Gly-hCAII) were prepared. A uniformly ^{15}N-labeled enzyme ([U-^{15}N]h-CAII) was obtained from a bacterial cell *E. coli* BL21(DE3) containing pET-hCAII gene and pLys-S plasmids grown in an enriched M9 medium with $^{15}NH_4Cl$. The pET-hCAII gene (24) was a generous gift from Prof. Sly (St. Louis University School of Medicine). All the isotopically labeled chemicals were purchased from Cambridge Isotope Laboratories.

Expression and Purification of Enzyme—The gene expression was induced by the addition of 1.2 mM isopropyl β-D-galactopyranoside and 1.2 mM $ZnSO_4$ upon reaching the log

TABLE 1
Parameters for NMR measurements and solution conditions

Experiment	Sample	Spectral widths (Hz)						Points			Phase delay or mixing time		H_2O:D_2O	pH	Ref. for pulse sequence
		f_1		f_2		f_3		t_1	t_2	t_3					
		Hz		Hz		Hz					ms				
$^{15}N/^{1}H$ HSQC[a]	[α-^{15}N]-His/[1-^{13}C]Gly–hCAII	^{15}N	800	^{1}H	6250			256	1024		N–H	2.25[b]	90:10	5.2	31
HNCO	[U-^{13}C/^{15}N]His–hCAII	^{15}N	800	^{1}H	6250			30	1024		N–H	2.25[b]	90:10	5.2	32
											C–H	13.5[b]			
HNCA	[U-^{13}C/^{15}N]His–hCAII	^{1}H	6250	^{13}C	1250	^{15}N	800	1024	36	32	N–H	2.25[b]	90:10	5.2	33
											N–C	13.5[b]			
HCCH	[U-^{13}C/^{15}N]His–hCAII	^{13}C	2500	^{1}H	6250			64	1024		C–H	1.80[b]	90:10	5.2	34
											C–C	5.00[b]			
(Hβ)Cβ(CγCδ)Hδ	[U-^{13}C/^{15}N]His–hCAII	^{13}C	2500	^{1}H	6250			32	1024		C–H	1.80[b]	90:10	5.2	35
											C–C	5.00[b]			
$^{15}N/^{1}H$ HSQC[c]	[*ring*-^{15}N]His–hCAII	^{15}N	8000	^{1}H	6250			256	1024		N–H	11.0[b]	90:10	5.2–9.0	31
$^{15}N/^{1}H$ HSQC[c]	[U-^{15}N]hCAII	^{15}N	8000	^{1}H	6250			256	1024		N–H	11.0[b]	90:10	5.2–9.0	31
$^{15}N/^{1}H$ HSQC[d]	[U-^{15}N]hCAII	^{15}N	8000	^{1}H	12500			256	4096		N–H	2.25[b]	90:10	5.2–8.8	31
NOESY	hCAII	^{1}H	16000	^{1}H	16000			64	2048		mix	100	90:10	6.9	36
$^{15}N/^{1}H$ HMQC-NOESY	[U-^{15}N]hCAII	^{15}N	6250	^{1}H	16000			256	2048		N–H	4.20[e]	90:10	6.9	37
											mix	50.0			
$^{13}C/^{1}H$ HSQC	[*ring*-Cε1-^{13}C]His–hCAII	^{13}C	1600	^{1}H	6250			96	1024		C–H	1.10[b]	0:100	4.7–9.3	31
$^{13}C/^{1}H$ HSQC	[*ring*-Cε1-^{13}C]His–apo-hCAII	^{13}C	1600	^{1}H	6250			96	1024		C–H	1.10[b]	0:100	4.7–9.3	31

[a] For the detection of amide N-H correlation cross-peaks.
[b] $1/(4J_{x\text{-}y})$.
[c] For the detection of imidazole $N^{\delta1}$-$H^{\delta2}$, $N^{\delta1}$-$H^{\epsilon1}$, $N^{\epsilon2}$-$H^{\delta2}$, and $N^{\epsilon2}$-$H^{\epsilon1}$ correlation peaks.
[d] For the detection of imidazole $N^{\delta1}$-$H^{\delta1}$ or $N^{\epsilon2}$-$H^{\epsilon2}$ correlation peaks.
[e] $1/(2J_{x\text{-}y})$.

phase (A_{600} = 0.6) in the growth curve. The cells were collected 16 h later and the harvest was extracted in 50 mM Tris sulfate, 0.1% Triton X-100, pH 8.0, after sonication. The enzyme was purified by affinity column chromatography as described by Osborne and Tashian (25), followed by gel filtration with Sephadex G-75. The purified sample was stored as a lyophilized powder at −20 °C. The zinc-free apoenzyme was prepared by treating the purified sample with pyridine-2,6-dicarboxylic acid (dipicolinic acid), according to Hunt *et al.* (26). Protein concentrations were determined by using the extinction coefficient $\epsilon = 54800\ M^{-1}\ cm^{-1}$ at 280 nm for hCAII (27). The purity was confirmed by reverse-phase high performance liquid chromatography on a C4-column (YMC Co.). The molecular weight (29,000) of native enzyme was confirmed by the sedimentation equilibrium method with an Optima XL-A (28). The enzyme activity was confirmed by the hydrolysis rate of 1 mM 4-nitrophenyl acetate (29, 30).

NMR Measurements—The lyophilized powder was dissolved in 20 mM acetate buffer with 200 mM Na_2SO_4, pH 5.2, to prepare 1.5 mM of the selectively labeled enzyme samples and 3.0 mM of the uniformly labeled enzyme sample. All NMR experiments ($^{15}N/^{1}H$ HSQC, $^{13}C/^{1}H$ HSQC, two-dimensional HNCO, three-dimensional HNCA, two-dimensional HCCH, and two-dimensional (Hβ)Cβ(CγCδ)Hδ) were carried out by a Bruker ARX-500 and/or AMX-500 spectrometer at 25 °C. The NMR parameters for this histidine study and the references for basic pulse sequences (31–37) are summarized in Table 1. In the $^{15}N/^{1}H$ HSQC experiments for imidazole analysis, we picked up a series of signals from [U-^{15}N]hCAII consistent with those from [*ring*-^{15}N]His-hCAII. Chemical shifts were referenced to internal 2,2-dimethyl-2-silapentane-1-sulfonate for ^{1}H and ^{13}C nuclei, and to external $^{15}NH_4Cl$ (2.9 mM in 1 M HCl at 25 °C) for the ^{15}N nucleus, which is 23.6 ppm downfield from liquid NH_3 (38).

Determination of Acid Base and Tautomeric Equilibrium Constants of Histidine—The imidazolium cation exists in an acid-base equilibrium with two neutral species. These neutral forms of imidazole, the $N^{\delta1}$-H tautomer and the $N^{\epsilon2}$-H tautomer, exist in tautomeric equilibrium. The acid-base equilibrium constants K_1 and K_2 are given by K_1 = ($N^{\delta1}$-H tautomer)(H^+)/(imidazolium cation) and K_2 = ($N^{\epsilon2}$-H tautomer)(H^+)/(imidazolium cation), whereas the tautomeric equilibrium constant K_T is given by K_T = ($N^{\delta1}$-H tautomer)/($N^{\epsilon2}$-H tautomer) (39). The experimentally determined value K_a is given by $K_a = K_1 + K_2$. The K_T and pK_a values of L-histidine are 0.25 and 6.2 in aqueous solution, respectively (40–42). The ^{15}N chemical shifts at various pH values are derived from the Henderson-Hasselbalch equation as,

$$\delta_N^{obs} = \delta_{>N(H)}^{basic}\frac{1}{1 + 10^{(pKa - pH)}} + \delta_{+>NH}^{acidic}\left(1 - \frac{1}{1 + 10^{(pKa - pH)}}\right) \quad \text{(Eq. 1)}$$

where δ_N^{obs} is the observed ^{15}N chemical shift. The limiting chemical shifts at basic and acidic pH are represented by $\delta_{>N(H)}^{basic}$ and $\delta_{+>NH'}^{acetic}$, respectively. Parameters $\delta_{>N(H)}^{basic}$, $\delta_{+>NH'}^{acetic}$, and K_a were determined by fitting Equation 1 to the experimental data using Kaleida Graph software (Synergy Software Co.). $\delta_{>N(H)}^{basic}$ is the population-weighted average value of the ^{15}N chemical shifts of pyrrole-like (>N-H) and pyridine-like (>N:) types; the proportion of $N^{\delta1}$-H or $N^{\epsilon2}$-H type nitrogen to the entire nitrogen, P($N^{\delta1}$-H or $N^{\epsilon2}$-H), is approximately expressed as a function of $\delta_{>N(H)}^{basic}$ as,

$$P = \frac{\delta_{>N} - \delta_{>N(H)}^{basic}}{\delta_{>N} - \delta_{>NH}} \quad \text{(Eq. 2)}$$

where $\delta_{>N\text{-}H}$ and $\delta_{>N}$ are ^{15}N chemical shifts of pyrrole-like (>N-H) and pyridine-like (>N:) nitrogen types, respectively. $\delta_{>N}$ and $\delta_{>N\text{-}H}$ are assumed to be 249.5 and 167.5 ppm, respectively. These values were derived from small model compounds (43). The tautomeric equilibrium constant K_T is given by the following equation.

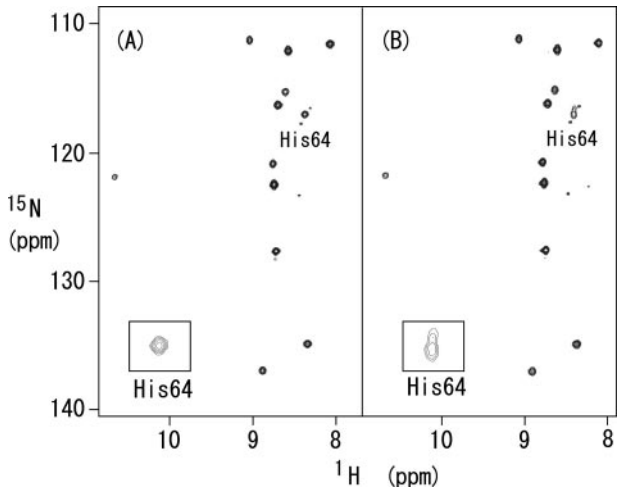

FIGURE 2. **The amide assignment of His^{64} in hCAII by using the double labeling method.** ^{15}N/^{1}H HSQC spectra of [α-^{15}N]His/[1-^{13}C]Gly-hCAII were obtained by the measurements (*A*) with decoupling (*B*) without decoupling the ^{13}C-carbonyl region during t_1 at pH 5.2 and 25 °C. A doublet (^{15}n = 117.2 ppm and ^{1}H = 8.41 ppm) in *B* was assigned to the His^{64} amide.

$$K_T = \frac{P_{N\delta 1-H}}{P_{N\epsilon 2-H}} \qquad \text{(Eq. 3)}$$

The procedure cannot be verified as being highly accurate, but certainly it is more accurate than any other determination for solutions, including the use of C-N coupling constants (44). When there is the expected 82-ppm chemical shift difference, even a 2–3 ppm uncertainty in the limiting shift values of the numerator in Equation 3 will allow quite reasonable estimates (±5%) of K_T. However, the same order of uncertainty in the denominator can cause a significant error, especially when the difference $\delta_{>N} - \delta_{>NH}$ in Equation 2 is very small, or the tautomerization is in favor of the N$^{\delta 1}$-H form.

RESULTS

Assignment of ^{1}H, ^{13}C, ^{15}N Signals of His^{64}—There is no strategy for the simple direct assignment of the imidazole ring within histidine residues. By combining a unique method of amide assignment and the following techniques of intra-residual assignment, we carried out the unambiguous imidazole assignment of His^{64} in hCAII. The double-labeling method (45) was applied to the amide assignment of His^{64}, which was performed by using a selectively labeled enzyme, [α-^{15}N]His/[1-^{13}C]Gly-hCAII. Among 12 histidine residues in hCAII, only His^{64} is linked to Gly; the peptidyl bond between Gly^{63} and His^{64} is labeled by both ^{15}N and ^{13}C. Twelve singlets of histidine resonances in the decoupling spectrum shown in Fig. 2*A* change into 11 singlets and one doublet in the non-decoupled spectrum shown in Fig. 2*B*. This spectral change clearly demonstrates that the doublet is due to His^{64}. This amide assignment was further confirmed in the two-dimensional HNCO spectrum of the same sample as shown in Fig. 3*A*. Fig. 3*B* shows the ^{13}C,^{1}H plane of the three-dimensional HNCA spectrum of [U-^{13}C/^{15}N]His-hCAII at ^{15}N = 117.2 ppm. The cross-peak between the amide proton and the Cα carbon of His^{64} was observed in the spectrum where Cα = 55.5 ppm. Fig. 3*C* shows the two-dimensional HCCH spectrum in which the

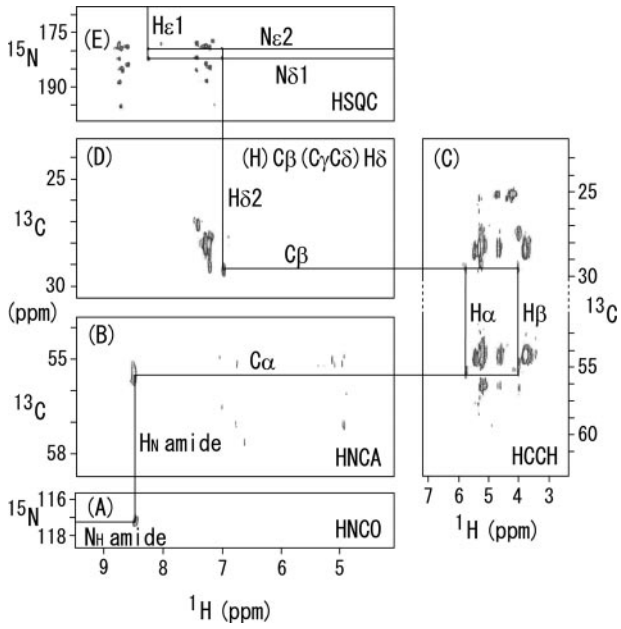

FIGURE 3. **The intra-residual assignment of His^{64} in hCAII.** *A*, HNCO spectrum of [α-^{15}N]His/[1-^{13}C]Gly-hCAII; *B*, HNCA; *C*, HCCH; and *D*, (Hβ)Cβ(CγCδ)Hδ spectra of [U-^{13}C/^{15}N]His-hCAII; and *E*, ^{15}N/^{1}H-HSQC spectrum of [U-^{15}N]hCAII at pH 5.2 and 25 °C. The connection from the amide nitrogen to imidazole nitrogen of His^{64} is emphasized by *solid lines*.

resonances of Cβ, Hα, and Hβ of His^{64} were observed at 29.3, 5.80, and 4.05 ppm, respectively. Fig. 3*D* shows the two-dimensional (Hβ)Cβ(CγCδ)Hδ spectrum to connect Cβ with H$^{\delta 2}$. The H$^{\delta 2}$ resonance of His^{64} was observed at 6.95 ppm. Fig. 3*E* shows the ^{15}N/^{1}H-HSQC spectrum of the [*ring*-^{15}N]His-hCAII at pH 5.2. In this spectrum, four correlation signals, N$^{\delta 1}$-H$^{\delta 2}$, N$^{\delta 1}$-H$^{\epsilon 1}$, N$^{\epsilon 2}$-H$^{\delta 2}$, and Nϵ2-H$^{\epsilon 1}$, per histidine residue are observed. When both N$^{\delta 1}$ and N$^{\epsilon 2}$ atoms are positively charged (designated as the +>N-H nitrogen type) in the imidazolium cation, the ^{15}N signals of N$^{\delta 1}$ and N$^{\epsilon 2}$ are observed around 176.5 ppm, with N$^{\delta 1}$ generally appearing at a ~2 ppm higher frequency than N$^{\epsilon 2}$ (40–43). The identification of N$^{\delta 1}$ and N$^{\epsilon 2}$ nuclei can be confirmed at basic pH regions. By gradually changing the pH from 5.2 to basic, one of their signal intensities change characteristically; the N$^{\delta 1}$-H$^{\delta 2}$ resonance weakens in intensity where the $^{3}J_{N\delta 1\text{-}H\delta 2}$ coupling is too small (−2 Hz) (46) to observe the resonance, as shown in Fig. 4. As a result, this weakening signal allows us to assign three other observable resonances, N$^{\delta 1}$-H$^{\epsilon 1}$, N$^{\epsilon 2}$-H$^{\epsilon 1}$, and N$^{\epsilon 2}$-H$^{\delta 2}$. Consequently, the H$^{\epsilon 1}$, N$^{\delta 1}$, and N$^{\epsilon 2}$ nuclei of His^{64} were assigned to the ^{1}H and ^{15}N chemical shifts of 8.03, 177.8, and 175.4 ppm, respectively, at pH 5.2. Venters and co-workers (47) have reported the backbone resonance assignment of hCAII-substituted non-exchangeable protons for deuterium to detect the signals of this large-size protein without overlap, in which there is not enough available chemical shift data of the resonance to confirm our amide assignment of His^{64}.

The Imidazole ^{15}N Signals and Proton-exchange Rate—The assigned imidazole ^{15}N signals of His^{64} can serve as a good probe that provides both the pK_a data and information concerning the tautomeric forms of this residue (K_T). Although the pK_a data could be obtained using the ^{1}H signal of H$^{\epsilon 1}$ (13), the ^{1}H signal cannot discriminate between two possible tautomers

of the imidazole ring. To determine the K_T value, it is essential to observe the ^{15}N signals of $N^{\delta1}$ and $N^{\epsilon2}$ simultaneously. The ^{15}N signals of the imidazole nitrogen nuclei characteristically reflect the charged states of the imidazole ring (43). In the cationic imidazolium form, both nuclei attached to protons showed a chemical shift at around 176.5 ppm. In the neutral form, $N^{\delta1}$- and $N^{\epsilon2}$-^{15}N exhibit signals at 167.5 ppm when these nitrogen atoms are protonated and at 249.5 ppm when they are not protonated, allowing us to distinguish between two tautomeric forms involving these nitrogen atoms. In favorable cases, these ^{15}N signals of $N^{\delta1}$ and $N^{\epsilon2}$ are observed in a "fast exchange" regime, where their signals are averaged to give a single resonance. Note that the rate of proton-exchange between these two nitrogen atoms is more than $1.6 \times 10^4\ s^{-1}$. When the proton prefers one of the nitrogen nuclei, the weight averaging of the chemical shifts occurs in the $N^{\delta1}$ and $N^{\epsilon2}$ signals.

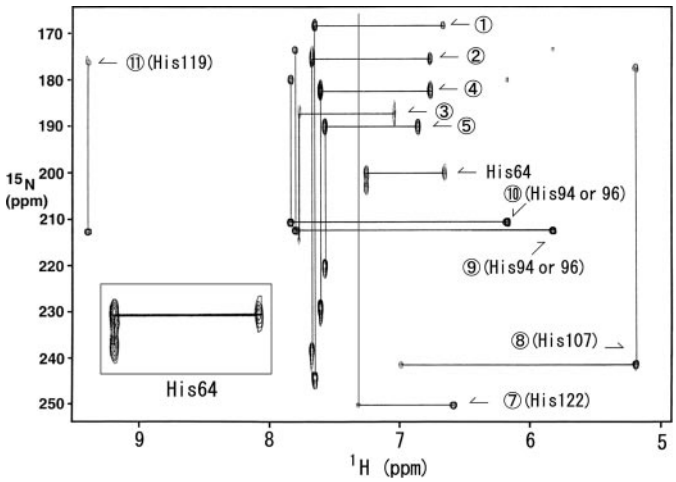

FIGURE 4. **The $^{15}N/^1H$ HSQC spectrum of [*ring*-^{15}N]His-hCAII at pH 7.9.** The *horizontal lines* show the ^{15}N chemical shifts of $N^{\epsilon2}$, whereas the *vertical lines* show the ^1H chemical shifts of $H^{\epsilon1}$. Curve number 6 is not observed at this pH. Zinc-bound histidine residues (His^{94}, His^{96}, and His^{119}) are distinguished from other histidine residues by using apoenzyme. Buried histidine residues are assigned using the crystal structure. These assignments except for His^{64} are shown by *brackets*.

For the observation of imidazole ^{15}N signals of His^{64} in hCAII, two-dimensional $^{15}N/^1H$-correlation spectroscopy was used, which detects the $N^{\delta1}$-$H^{\epsilon1}$, $N^{\delta1}$-$H^{\delta2}$, $N^{\epsilon2}$-$H^{\epsilon1}$, and $N^{\epsilon2}$-$H^{\delta2}$ resonances described above. As shown in Fig. 4, the signals of His^{64} were observed to be regarded as "fast" at pH 7.9. In this measurement, all other imidazole ^{15}N signals except the signal number 6 were also observed as the fast exchange. For signal number 6, considering the signals to be observed in the region of pH 5.2–6.7, one of the exchange rates may change from fast to "intermediate" with increasing pH. However, for this signal disappearance, this could not be concluded easily because the signal intensity is related not only to the exchange, but also to some other factors such as *J*-coupling constants dependent on pH.

The pH Dependence and Tautomeric Proportion of Histidine Residues—^{15}N chemical shifts were monitored as a function of pH to investigate the profile of acid-base and tautomeric equilibrium of the histidine residue. The pH-titration curves of $N^{\delta1}$ and $N^{\epsilon2}$ for all 12 histidine residues are shown in Fig. 5. To simply illustrate the pH dependence of the ^{15}N chemical shift, the variation of the ^{15}N chemical shifts with pH are simulated by substituting the pK_a value of L-histidine (6.2), the chemical shift value of the +>N-H type, and the variable weight average of >N-H and >N: chemical shifts for Equations 1–3, as shown in Fig. 6. This figure allows us to facilitate the investigation of the tautomeric proportion in histidine residues under the fast exchange situation. Comparing Figs. 5 and 6, the approximate K_T values of the histidine residues are quite obvious. In the case of pH-independent ^{15}N chemical shifts, their titration curves need not be compared with that of Fig. 6. In both cases, the K_T values were calculated by Equations 2 and 3 using the basic ^{15}N-limitting shift. Table 2 summarizes the acid-base and tautomeric equilibrium constants of the histidine residues.

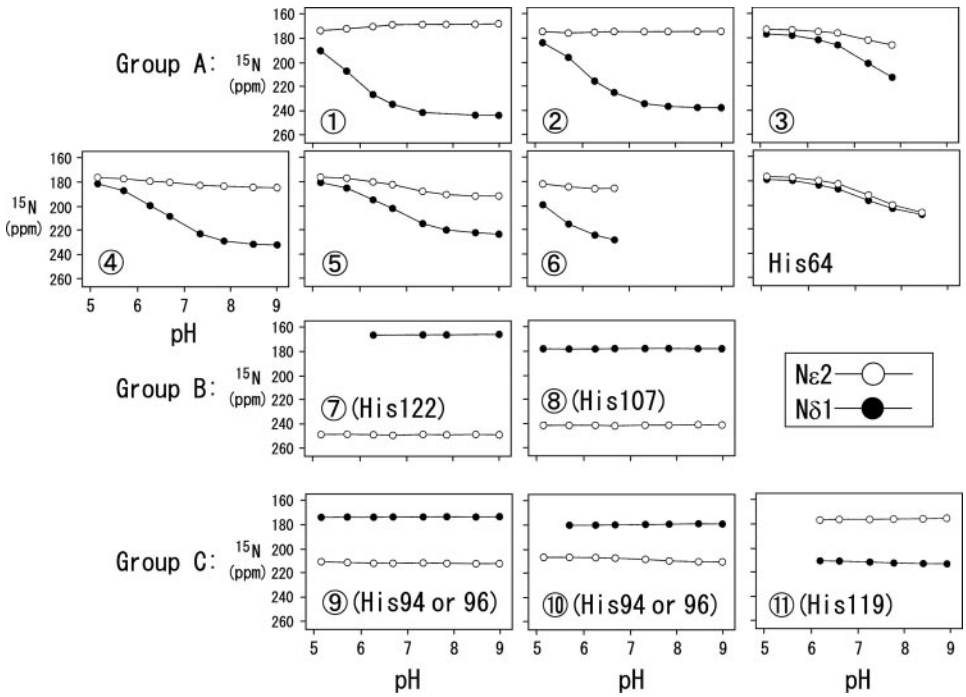

FIGURE 5. **The pH-titration curves of $N^{\delta1}$ and $N^{\epsilon2}$ of histidine residues of hCAII.** The tautomeric equilibrium constant K_T of each histidine residue was determined by comparing the dependence of a pair of titration curves with the simulated ones shown in Fig. 6. Those for histidine residues with pH-independent profiles were directly obtained from Equations 2 and 3.

According to their titration profiles, histidine residues of hCAII were classified into three groups, A, B, and C, as summarized in Table 2. Group A consists of seven histidine residues sensitive to the tested pH changes (Group A: the change between acid and base limiting shift values is >30 ppm for either $N^{\delta1}$ or

$N^{\epsilon 2}$). These histidine residues would be distributed on the surface or in a solvent-accessible position in the molecule. For this study, one of them was unambiguously assigned to His^{64} as described above. His^{64} occurs in the equivalent proportion of the tautomer: $K_T = 1.0$. To our knowledge, no behavior similar to that of His^{64} has been found in any other protein. The six other histidine signals are designated as 1–6. The K_T constants are found to be in the range from 0.01 to 0.4. Curves 1 and 2 show that the hydrogen atoms are localized on $N^{\epsilon 2}$ of their histidine residues, whereas curves 3–6 show normal tautomeric profiles, similar to that of L-histidine amino acid in aqueous solution. These histidine residues are thought to be on the surface of the molecule. Group B consists of two pH-insensitive histidines, designated as 7 and 8 (Group B: the change between acid and base limiting shift values is <0.1 ppm for both $N^{\delta 1}$ and $N^{\epsilon 2}$). The $N^{\delta 1}$ signals of 7 and 8 appeared as >N-H type, and the $N^{\epsilon 2}$ signal as the >N: type, thus indicating that these histidine residues exist as $N^{\delta 1}$-H tautomers in all pH values tested. Group C consists of three slightly pH-sensitive histidines designated as curves 9–11 (Group C: the change between acid and base limiting shift values is between 0.5 and 5 ppm for either $N^{\delta 1}$ or $N^{\epsilon 2}$). The $N^{\delta 1}$ of 9 and 10, and $N^{\epsilon 2}$ of 11 appear as >N-H types. This result shows that 9 and 10 histidines occur as $N^{\delta 1}$-H tautomers; $N^{\delta 1}$ of 9 experiences a 7 ppm low field chemical shift change compared with typical pyrrole-like (>N-H) nitrogen and $N^{\delta 1}$ of 10 at 12.5 ppm. Number 11 of the histidine residue behaves like a $N^{\epsilon 2}$-H tautomer; $N^{\epsilon 2}$ is a 9.5-ppm low field chemical shift change.

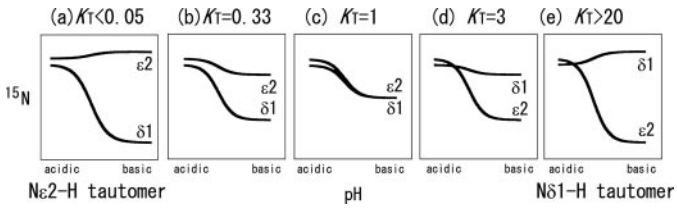

FIGURE 6. **The schematic pH-titration curve related to the tautomeric equilibrium constant of the histidine residue.**

Identifications and Assignments of Zinc-bound and Buried Histidine Residues—Crystal structure shows two kinds of interior or not exposed histidine residues: zinc-bound histidines, His^{94}, His^{96}, and His^{119}, and buried histidines, His^{107} and His^{122} (12). These residues except for His^{122} are illustrated in Fig. 1. First, we distinguished the zinc-bound histidines from the buried histidines by comparing the $C^{\epsilon 1}$-$H^{\epsilon 1}$ correlation signal of the holoenzyme with that of the apoenzymes. The pH titration experiment was carried out on [*ring*-$C^{\epsilon 1}$-^{13}C]His-hCAII using $^{13}C/^{1}H$ HSQC experiments. The $H^{\epsilon 1}$ titration profiles are consistent with those from the $^{15}N/^{1}H$ experiments described above; the pK_a values and chemical shift values of $H^{\epsilon 1}$ were confirmed. Fig. 7, *A* and *B*, shows the spectra of holo- and apoenzymes labeled with [*ring*-$C^{\epsilon 1}$-^{13}C]His at pH 7.0. Comparing them, the His^{64} signal and three other signals (numbers 9–11) disappear from the spectrum of the apoenzyme. Instead of these signals, several other signals appear. This observation shows that signals 9–11 were from three zinc-bound imidazoles of the histidine residues. This result is consistent with that of the above described ^{15}N experiment in which either a $N^{\delta 1}$ or $N^{\epsilon 2}$ signal is observed in the region between 205 and 215 ppm, which is of the zinc-bound nitrogen type (48). Subsequently, we tentatively assigned signals 9–11 to the zinc-bound histidine residues by using the crystal structure of enzyme. Among the three His residues coordinated with the zinc ion, His^{119} is

TABLE 2
Constants and titration profile for histidine residues

Group	Residual or signal number[a]	K_T (±5%)	Nucleus	pK_a (±0.1)	Limiting shift (ppm)	$^{1}J_{NH}$
						Hz
A	1	<0.05	$N^{\delta 1}$	5.8	179.0–243.5	
			$N^{\epsilon 2}$	5.9	174.6–168.2	
	2	0.1	$N^{\delta 1}$	6.1	177.2–238.1	
			$N^{\epsilon 2}$	ND[b]	174.6–168.2	
	3	0.4	$N^{\delta 1}$	7.3	177.8–222.9	
			$N^{\epsilon 2}$	7.3	173.8–190.3	
	4	0.3	$N^{\delta 1}$	6.6	179.4–230.6	
			$N^{\epsilon 2}$	6.6	175.1–182.7	
	5	0.4	$N^{\delta 1}$	6.6	178.9–222.0	
			$N^{\epsilon 2}$	6.8	174.7–191.0	
	6	0.3	$N^{\delta 1}$	5.3	177.1–229.8	
			$N^{\epsilon 2}$	5.0	174.9–185.3	
	His^{64}	1.0	$N^{\delta 1}$	7.2	178.2–208.3	
			$N^{\epsilon 2}$	7.3	175.8–207.7	
B	7 (His^{122})	$N^{\delta 1}$-H	$N^{\delta 1}$		167.8–167.8	93–96 ($^{1}J_{N\delta 1\text{-}H\delta 1}$)
			$N^{\epsilon 2}$		249.3–249.3	
			$H^{\delta 1}$		10.1–10.1	
	8 (His^{107})	$N^{\delta 1}$-H	$N^{\delta 1}$		177.5–177.5	91–94 ($^{1}J_{N\delta 1\text{-}H\delta 1}$)
			$N^{\epsilon 2}$		240.5–240.5	
			$H^{\delta 1}$		14.3–14.3	
C	9 ($His^{94/96}$)	$N^{\delta 1}$-H	$N^{\delta 1}$		174.5–174.5	92–97 ($^{1}J_{N\delta 1\text{-}H\delta 1}$)
			$N^{\epsilon 2}$(Zn)	ND[b]	212.0–212.5	
			$H^{\delta 1}$	7.3 ± 0.04	12.8–12.7	
	10 ($His^{94/96}$)	$N^{\delta 1}$-H	$N^{\delta 1}$		180.0–180.0	92–97 ($^{1}J_{N\delta 1\text{-}H\delta 1}$)
			$N^{\epsilon 2}$(Zn)	ND[b]	207.5–211.5	
			$H^{\delta 1}$	7.2 ± 0.02	13.9–13.7	
	11 (His^{119})	$N^{\epsilon 2}$-H	$N^{\delta 1}$(Zn)	ND[b]	211.0–211.5	
			$N^{\epsilon 2}$		177.0–177.0	92–93 ($^{1}J_{N\epsilon 2\text{-}H\epsilon 2}$)
			$H^{\epsilon 2}$	7.2 ± 0.03	15.2–14.8	

[a] Numbers 1–6 histidine residues are located on the surface of molecule, which includes histidines 3, 4, 10, 15, 17, and 36. The number 1 or 2 may be from His^{15} (see also "Discussion"). His^{64} is assigned using unique NMR techniques. The residues in parentheses are tentatively assigned using crystal structure.
[b] ND, not determined.

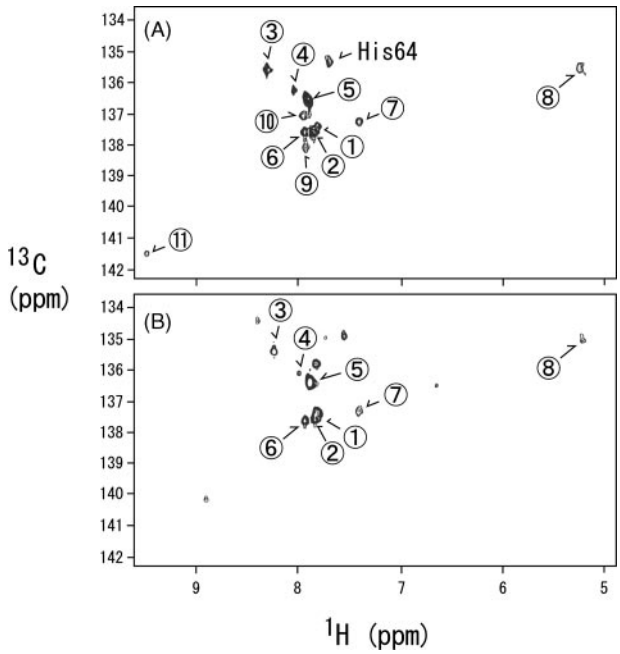

FIGURE 7. *A*, the $^{13}C/^{1}H$ HSQC spectrum of holo-hCAII selectively enriched with [*ring*-$C^{\epsilon 1}$-^{13}C]His at pH 7. 0 and 25 °C where all 12 histidine signals were obtained. *B*, the $^{13}C/^{1}H$ HSQC spectrum of apo-hCAII at the same condition. Four signals (numbers 9–11, and His^{64}) disappeared compared with *A*. Instead of these signals, two sharp signals and several weak signals were observed. In these spectra, numbers 9–11 were identified with zinc-bound histidine residues.

unique in that its $N^{\delta 1}$ is coordinated with the zinc, whereas His^{94} and His^{96} are coordinated with the zinc via their $N^{\epsilon 2}$ atoms, thus, number 11 would be assigned to the imidazole of His^{119}. The $H^{\epsilon 1}$ atom of His^{119} exists in the plane of the indole ring of Trp^{209}. The ring current effect of Trp^{209} is expected to bring about the low field chemical shift change of the $H^{\epsilon 1}$. In fact, the $H^{\epsilon 1}$ nucleus of number 11 was observed at 9.3 ppm. Numbers 9 and 10 are assigned to either the zinc-bound imidazole of His^{94} or His^{96} (these are designated as $His^{94/96}$). In the buried histidine residues, His^{107} exists in the plane perpendicular to the indole ring of Trp^{209}, in contrast to His^{119}. The upfield chemical shift of the $H^{\epsilon 1}$ observed in the spectra is 5.1 ppm of number 8, and thus, number 8 would be assigned to His^{107}. The remaining signal of number 7 would be assigned to His^{122}.

Direct Observation of Protons Fixed on Nitrogen within the Imidazole Group of Histidine Residues—Although, at a higher pH value than 2.0, an imidazole H_N ($H^{\delta 1}$ or $H^{\epsilon 2}$) signal is not observed because of the exchange of imidazole H_N with the proton of bulk water, the imidazole H_N shows its signal for a fixed or hydrogen-bonded proton in the downfield region around 13.5 ppm. Five signals were observed in this region of the $^{15}N/^{1}H$ HSQC spectrum for the ^{15}N-labeled enzyme, as shown in Fig. 8*A*. All five ^{15}N chemical shifts correspond with those of the above described >N-H type nitrogen of either Group B ($N^{\delta 1}$ of His^{122} and $N^{\delta 1}$ of His^{107}) or C ($N\delta 1$ of $His^{94/96}$ and $N^{\epsilon 2}$ of His^{119}), whereas no signal corresponds with the nitrogen of Group A (surface and His^{64}). The imidazole H_N assignment is supported by an additional NOE cross-peak (49). The NOE cross-peaks for $H^{\delta 1}$ of His^{107}, $H^{\delta 1}$ of $His^{94/96}$, and $H^{\epsilon 2}$ of His^{119} were confirmed by using the NOESY as shown in Fig. 8*B*. For $H^{\delta 1}$ of His^{122}, the NOE cross-peak was confirmed by using $^{15}N/^{1}H$ HMQC-NOESY as shown in Fig. 8*C*. The H_N chemical shifts are added to Table 2. Scalar spin-spin coupling constants ($^{1}J_{NH}$) of the N-H bonds of the imidazole ring are summarized in Table 2. The values of $^{1}J_{NH}$ provides a direct measure of covalent bond character; the observed values of 92–97 Hz indicate that these imino protons are fixed covalently about 90–100% (50).

The H_N chemical shifts were monitored as a function of pH to calculate pK_a values. In the ^{15}N-labeled enzyme, all five H_N signals were observed in the region of pH 5.7–8.8. All H_N chemical shifts were slightly sensitive to pH change, as shown in Fig. 8*D*. For Group B, the H_N signal of His^{107} ($H^{\delta 1}$) shifts to a slightly lower field as the pH increases, which is different from the pH dependence of zinc-bound histidine residues in the direction of shift. The titration curve does not exhibit sigmoid behaviors and the difference between chemical shifts at acidic and basic is very small, 0.06 ppm. The H_N signal of His^{122} ($H^{\delta 1}$) shifts to a slightly higher field. In the $H^{\delta 1}$ of $His^{94/96}$ and $H^{\epsilon 2}$ of His^{119} of Group C, the titration curves exhibited the clearly sigmoid behaviors dependent on pH required to calculate pK_a values and limiting shifts using δ^{obs} of the proton instead of δ_N^{obs} in Equation 1. The pK_a values of $H^{\delta 1}$ of $His^{94/96}$ (number 9), $H^{\delta 1}$ of $His^{94/96}$ (number 10), and $H^{\epsilon 2}$ of His^{119} are 7.3 ± 0.04, 7.2 ± 0.02, and 7.2 ± 0.03, respectively. The pK_a values of His^{94}, His^{96}, and His^{119} probably reflect the titration behavior of other residues or groups because these residues are unattached to water molecules. Importantly, these pK_a values are in good agreement with that of His^{64} determined in our measurements. The coincidence implies that the titration behavior of His^{64} is reflected on those of zinc-bound histidine residues. However, the possibility that the observed effect is due to the ionization of zinc-bound water could not be ruled out.

DISCUSSION

Implication of Tautomeric Equilibrium Constant of Histidine Residues—We determined the tautomeric equilibrium constant (K_T) of the imidazole ring of His^{64} to be 1.0, according to the unambiguous assignment of ^{15}N signals, the analysis of their pH dependences, and a comparison of experimental and simulated titration curves. This value was different from those of 11 other histidine residues in this enzyme, whereas its pK_a value of 7.2–7.3 was indistinguishable from those of the others (Table 2). The K_T value of 1.0 indicates that two imidazole nitrogen atoms ($N^{\delta 1}$ and $N^{\epsilon 2}$) can be equally involved in the catalytic reaction. It is therefore reasonable to assume that one of the imidazole nitrogen atoms acts as a general acid, whereas the other acts as a general base, as shown in Equation 4.

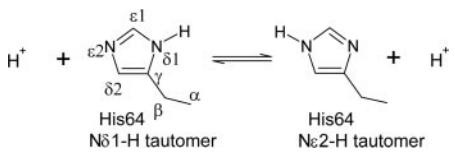

(Eq. 4)

Because the tautomeric equilibrium of an imidazole group is dominated by hydrogen bond interactions with the δ1-nitrogen where an acid or base interacts strongly, the usual equilibrium condition gives a large deviation of the K_T values from 1 (51).

For example, the $N^{\delta 1}$-H tautomer dominates in the imidazole group of *cis*-urocanic acid, as indicated by $K_T = 5.2$ (Equation 5), in which the intramolecular hydrogen bond can be formed, whereas the $N^{\epsilon 2}$-H tautomer is favorable in Equation 6 with the *trans*-configuration preventing the hydrogen bond though a carboxylate anion ($K_T = 0.37$).

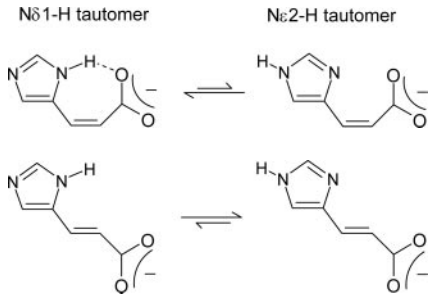

(Eq. 5)

(Eq. 6)

These K_T values suggest that the imidazole group intrinsically tends to be the $N^{\epsilon 2}$-H tautomer, unless a hydrogen bond interacts with the δ1-nitrogen of the imidazole ring. In fact, the K_T values for 6 histidine residues exposed to the solvent (Group A in Table 2) were shown to be less than 0.4, indicating the prevalence of the $N^{\epsilon 2}$-H tautomer.

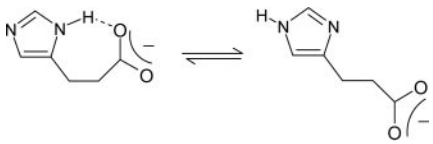

(Eq. 7)

As shown in Equation 7, the conformational flexibility along the Cβ-Cγ bond of 3-(imidazol-4-yl)propionic acid permits the partial formation of a hydrogen bond. In this case, the $N^{\epsilon 2}$-H tautomer still dominates, as in Equation 6, but the equilibrium shifts in favor of the $N^{\delta 1}$-H tautomer ($K_T = 0.61$). Based on this analogy, His^{64} should have a structure-specific determinant to promote the partial formation of a hydrogen bond. As illustrated in Equation 8, we consider that a negative charge of the zinc-bound hydroxide ion is responsible for increasing the population of the $N^{\delta 1}$-H tautomer, and a network of water molecules is responsible for attenuating the hydrogen bonding effect to a level comparable with that of the counterpart.

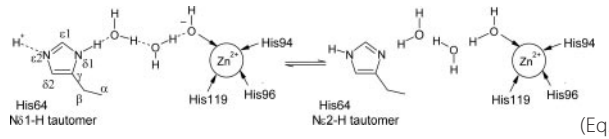

(Eq. 8)

Using this equation, we could consider that the tautomerization of His^{64} would be coupled to the ionization of the zinc-bound solvent.

To our knowledge, no real compound model has been reported to explain the ε2-nitrogen of an imidazole group in hydrogen bond interactions. In this case, we assumed that a hydrogen bond partner in close proximity to the ε2-nitrogen affects the change in the K_T value, in contrast to the δ1-nitrogen case as described above, is expected to decrease to much less than 0.4. This implies that one of the K_T values in Group A, <0.05 of signal number 1 or 0.1 of number 2, is from His^{15} because the ε2-nitrogen of His^{15} can form a hydrogen bond with oxygen of Lys-9 as a acceptor (distance: 3.19 Å), which may stabilize the $N^{\epsilon 2}$-H tautomeric form. For His^{107} and His^{122} in Group B, two hydrogen bond interactions are seen in the imidazole group, as shown in Fig. 8*E*, *a* and *b*, respectively. The conditions of His^{107} and His^{122} existing in a hydrogen bond network are apparently similar. Based on the structures, both histidine residues should take only the $N^{\delta 1}$-H tautomer. This is also supported by our measurement for *J* values, in which the $J_{N\delta 1\text{-}H\delta 1}$ value of His^{107} is close to that of His^{122}, indicating that hydrogen localization on the imidazole nitrogen of His^{107} is essentially equal to that of His^{122}. However, the apparent K_T values, 7.6 for His^{107} and >20 for His^{122}, were calculated by Equations 2 and 3, although a small error contained in the difference $\delta_{>N} - \delta_{>NH}$ in Equation 2 could make the comparison between their K_T values difficult. For the difference of these histidine residues, it is possible to argue the difference of their strengths of hydrogen bonds in terms of chemical shift values. Comparing Fig. 8*E*, *a* and *b*, we note that the distance of hydrogen bond between $N^{\delta 1}$ of His^{122} and the carbonyl oxygen of Ala^{142} (3.12 Å) is appreciably longer than that between δ1-nitrogen of His^{107} and the carboxyl oxygen of Glu^{117} (2.84 Å). Similarly, there is a slight increase in distance between the δ1-nitrogen of His^{122} and the hydroxyl oxygen of Tyr^{51} (2.78 Å) compared with that between the δ1-nitrogen of His^{107} and the hydroxyl oxygen of Tyr^{194} (2.66 Å). Such an increase in distances could lead to a weakening of hydrogen bond. In the $N^{\delta 1}$-H tautomer illustrated in Fig. 8*E*, *a*, the chemical shift values of $N^{\delta 1}$ (177.5 ppm) and $N^{\epsilon 2}$ (240.5 ppm) for His^{107} agree well with the expected limiting shifts due to donation (+10 ppm) and acceptance (−10 ppm) of hydrogen bonds, respectively (43, 52). Using these limiting shifts, the K_T value for His^{107}, >20, is determined by the calculation using Equations 2 and 3, taking only $N^{\delta 1}$-H tautomer. In contrast, the corresponding values of $N^{\delta 1}$ (167.8 ppm) and $N^{\epsilon 2}$ (249.3 ppm) for His^{122} do not accord with the above empirical rule, but appear to be independent of the hydrogen bonds with Tyr^{51} and Ala^{142}. That is, assume that neither δ1- nor ε2-nitrogen atoms of His^{122} is firmly involved in the hydrogen bond interactions but the ε2-nitrogen is rather involved in hydrogen bond interaction with the hydroxyl oxygen of Tyr^{51} because the slight or partial negative charge of the carbonyl oxygen of Ala^{142} can likely balance with the amide of His^{122}. For His^{122}, thus, the limiting shifts without the hydrogen bond, 167.5 and 249.5 ppm, are used to determine its K_T value, >20, taking only the $N^{\delta 1}$-H tautomer. For Group C, because of zinc coordination and hydrogen bonding, His^{94}, His^{96}, and His^{119} would exist only in one tautomeric form. Although their N_H chemical shifts are ~10 ppm lower than a typical chemical shift, 167.5 ppm, the imidazole N-H spin-coupling constants range from 90 to 98 Hz. Therefore the $H^{\delta 1}$ protons of His^{94} and His^{96} and the $H^{\epsilon 2}$ of His^{119} are essentially 100% localized on these nitrogen atoms, based on their one-bond *J* coupling constants.

Catalytic Mechanism of Carbonic Anhydrase II—It has been accepted that protonation of the $N^{\delta 1}$ of His^{64} results from the ionization of the water molecule to generate the hydroxide ion near the zinc ion, as shown in Equation 9 (5).

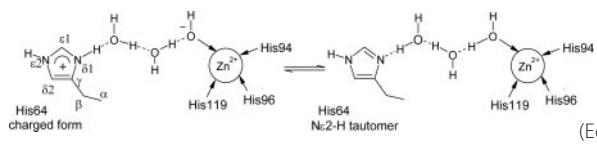

(Eq. 9)

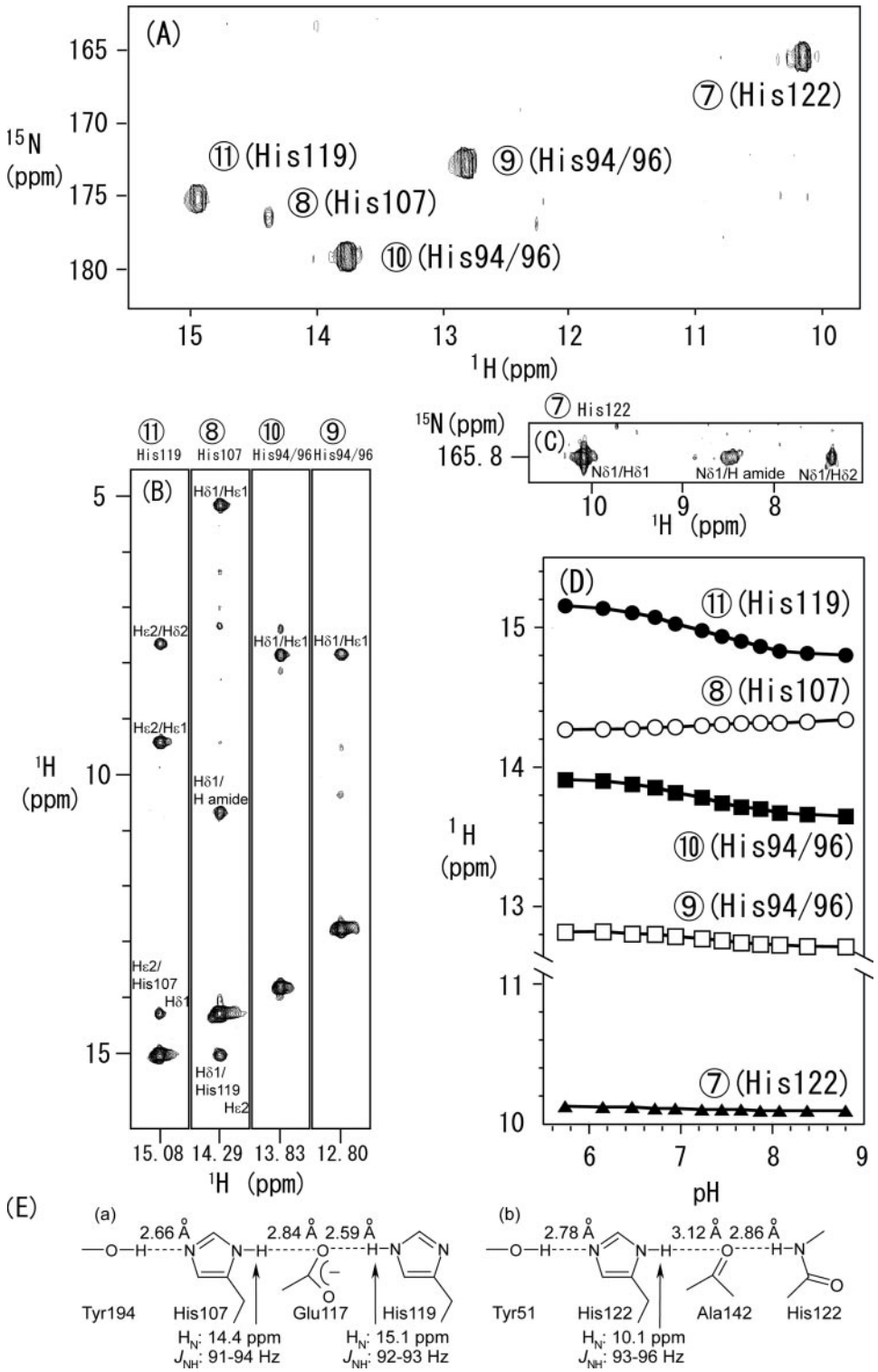

FIGURE 8. *A*, the ^{1}H low field region of the ^{15}N/^{1}H HSQC spectrum of U-^{15}N-labeled- hCAII at pH 7.5 to observe the $H^{\delta1}$ or $H^{\epsilon2}$ protons (H_N) of histidine residues. Signal numbers *7–10* ($His^{94/96}$, His^{107}, and His^{122}) are the $N^{\delta1}$-$H^{\delta1}$ cross-peak, and *11* (His^{119}) is the $N^{\epsilon2}$-$H^{\epsilon2}$ cross-peak. *B*, strips of the two-dimensional NOESY spectrum of hCAII at pH 6.9. The assignments of the cross-peaks are shown, except for His^{122}. *C*, the ^{15}N/^{1}H HMQC-NOESY spectrum of U-^{15}N-labeled hCAII at pH 6.9. The assignment of His^{122} is shown. *D*, the pH titration curves of the H_N protons. The pK_a values, 7.2–7.3, of the zinc-bound histidine residues are consistent with that of His^{64}. *E*, the profiles of hydrogen bond interactions around His^{107} (*a*) and His^{122} (*b*).

The protonation of δ1-nitrogen is confirmed to be appropriate because transfer of the proton was achieved by a concerted process in a dynamics study (53). Using this process, the intramolecular proton transfer step could be said to occur in the active site. However, this equation is limited for explaining the release of the proton into the bulk solution in the catalytic reaction, because the proton travels only inside the water bridge between His^{64} and the zinc ion like a shuttle, and it cannot jump from the water bridge to bulk solvent. For the proton release, a crystallographic study has proposed the swinging mechanism of His^{64}, as depicted in Fig. 1: that the productive proton transferred to the δ1-nitrogen of His^{64} is released from its nitrogen to the bulk solution after swinging (16). Although this mechanism is plausible, note that the swinging rate of the imidazole ring is considered to be the same as the rotation rate of the ring, such as the side chain of Phe or Tyr, to explain why the rate is comparable with the effective turnover (10^6 s^{-1}) of this enzyme. This analogy cannot be appropriate because the imidazole hydrogen bond ability of the ring and rotational symmetry are quite different from those of phenyl or hydroxyl-phenyl rings. Therefore, using the out conformation resulting from the imidazolium ion in the next reaction step was a problem. This problem has made it exceedingly difficult to reveal a reasonable pathway to transfer the productive proton via His^{64} in the proposed proton release mechanism, in view of the vague or indistinguishable tautomerization.

Here we clearly demonstrate the relation between His^{64} structures and the proton release in the catalytic reaction of hCAII. Using two neutral tautomers, the imidazole ring of His^{64} need not swing to transfer the productive proton in the reaction because the imidazolium cation is thought to be a transient intermediate in mediating the tautomerization, assuming that this intermediate is different from the out conformation of imidazolium in the character of its structure. Instead of swinging, we notice a variety of water molecule locations in the active site in crystal structures of hCAII. The relationship between the variation of water molecule locations and

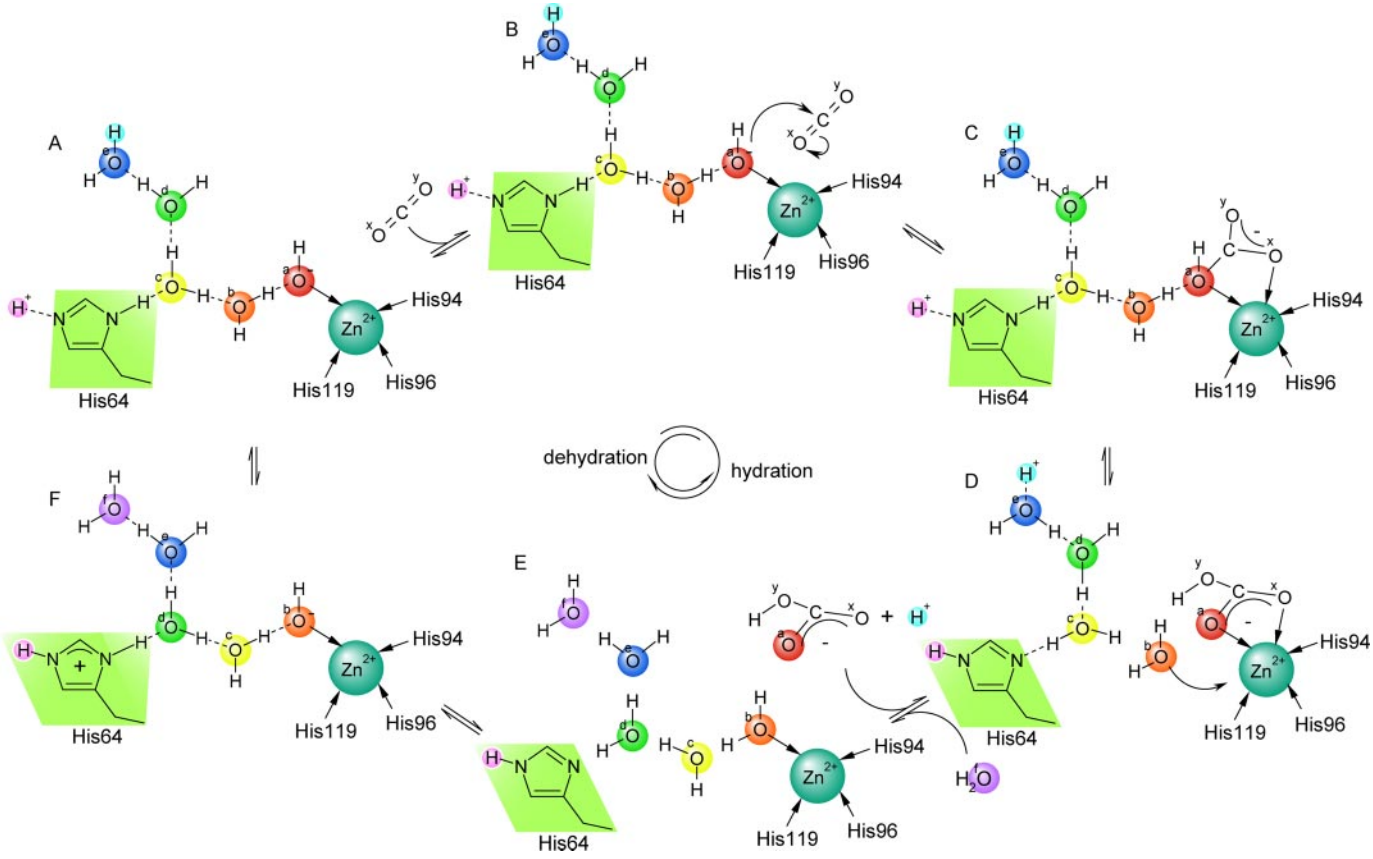

FIGURE 9. **A model for hydration or dehydration reactions in hCAII at a neutral pH.** The scheme exhibits the reaction through a flow of water molecules to continuously transfer protons; oxygen atoms are colored to emphasize the flow. Tautomerization of His^{64} can mediate the exchange of protons and water molecules between the bulk and the water bridge at the catalytic center, which suggests that it does not require any time- or energy-consuming process (see also "Discussion").

the reaction (Scheme 1) makes it reasonable that the water bridge (Fig. 1) can split in a process such as isomerization of a zinc-bound bicarbonate ion (54, 55) or the exchange of the product bicarbonate ion with a water molecule in the reaction. This indicates that a flow of the water molecules should occur in the active site to continue the reaction. We consider that behavior of water molecules such as the split and flow would occur within the $N^{\epsilon 2}$-H tautomer without hydrogen bond interaction, as shown in Fig. 9. In this scheme, the CO_2 hydration reaction proceeds in the following steps. 1) The zinc-bound hydroxide makes a direct nucleophilic attack on the carbonyl carbon of substrate CO_2 (Fig. 9, *A* and *B*). 2) This attack forms a zinc-bound bicarbonate intermediate in the active site (Fig. 9, *B* and *C*). 3) The bicarbonate intermediate isomerizes into the productive complex to be replaced with the solvent molecule shown as *B*, resulting in a split of the water bridge between His^{64} and the zinc ion. This split changes the $N^{\delta 1}$-H tautomer of His^{64} into the $N^{\epsilon 2}$-H tautomer via the transient imidazolium intermediate, which triggers the release of the product proton (shown in *light blue*), resulting in proton transfer among His^{64}, $H_2{}^cO$, $H_2{}^dO$, and $H_2{}^eO$ in that order (Fig. 9, *C* and *D*). In this step, we adopted the Lipscomb model for isomerization of the bicarbonate ion on the zinc ion according to the recent papers (54, 55). However, this does not necessarily give it any preference to the Linskog model; our scheme might not depend on the isomerization mechanism of the bicarbonate ion. 4) Releasing the product bicarbonate from the active site center, the water molecules remaining in the cave move into beside the zinc ion to reconstitute the water bridge, to which a brand new water molecule, shown as $H_2{}^fO$, is supplied from the bulk solution (Fig. 9, *D* and *E*). 5) Immediately, the zinc electric repulsion causes rapid ionization into the hydroxyl ion. This ionization would be coupled to the tautomerization of His^{64} (Fig. 9, *E* and *F*). Through the reconstituted water bridge, the protons transfer from the zinc-bound site to His^{64} where transferring protons would be achieved by a concerted process (53). 6) The regeneration of the initial mode is achieved by proton release from the ϵ2-nitrogen of His^{64} to the bulk solvent (Fig. 9, *F* and *A*), leading to the subsequent cycle of the catalytic reaction. Thus, this scheme explains the effective proton release following the intra-molecular proton transfer step in the catalytic reaction of hCAII. This scheme can be also used to explain the unique pH-dependent activity (9, 56, 57) of this enzyme, which has its maximum activity in pH 7. First, lowering pH accelerates that His^{64} would not participate in the hydrogen-bonded pathway because this residue takes the out conformation at low pH regions as shown in Fig. 1. This implies that the productive protons are transferred by another hydrogen-bonded pathway without His^{64}. Using this alternative pathway would decrease the proton transfer ability. Second, increasing pH would inhibit the addition of the proton (shown in *pink*) to the ϵ2-nitrogen of His^{64} in the *C*–*D* step in Fig. 9, or it might accelerate the

replacement of some water molecules between the zinc ion and His^{64} with hydroxyl ions. The loss of their protons may decrease the effective transfer of the productive proton by tautomerization of His^{64}.

In this study, our heteronuclear NMR approach to His^{64} shows that both the $N^{\delta 1}$-H and $N^{\epsilon 2}$-H tautomeric forms in equilibrium with an imidazolium ion are in the same population, providing information about the general acid-base function of the imidazole nitrogen. Here, we demonstrate a proton release model using the tautomeric information of His^{64}, implying a new insight into the catalytic mechanism for the hydration or dehydration reaction in human carbonic anhydrase II, *i.e.* the split of the water bridge and the flow of water molecules.

Acknowledgments—We thank Professor William S. Sly (St. Louis University School of Medicine) for the generous gift of the recombinant gene. We also thank Dr. Akiko Nishimura (National Institute of Genetics) for kindly providing the glycine auxotroph IQ417. Thanks are also due to Judith Steeh (Head Editor, Technical Communication Program in JAIST) and Dr. Evelyn R. Stimson for reading the text in its original form. We also thank an anonymous reviewer, who scrutinized the manuscript very carefully and gave us invaluable suggestions.

REFERENCES

1. Lindskog, S. (1997) *Pharmacol. Ther.* **74,** 1–20
2. Chegwidden, W. R., Carter, N. D., and Edwards, Y. H. (eds) (2000) *The Carbonic Anhydrases: New Horizons*, Birkhäuser Verlag, Basel, Switzerland
3. Earnhardt, J. N., Qian, M., Tu, C., Lakkis, M. M., Bergenhem, N. C., Laipis, P. J., Tashian, R. E., and Silverman, D. N. (1998) *Biochemistry* **37,** 10837–10845
4. Christianson, D. W., and Fierke, C. A. (1996) *Acc. Chem. Res.* **29,** 331–339
5. Christianson, D. W., and Cox, J. D. (1999) *Annu. Rev. Biochem.* **68,** 33–57
6. Steiner, H., Jonsson, B. H., and Lindskog, S. (1975) *Eur. J. Biochem.* **59,** 253–259
7. Tu, C. K., Silverman, D. N., Forsman, C., Jonsson, B. H., and Lindskog, S. (1989) *Biochemistry* **28,** 7913–7918
8. Taoka, S., Tu, C., Kistler, K. A., and Silverman, D. N. (1994) *J. Biol. Chem.* **269,** 17988–17992
9. Duda, D., Tu, C., Qian, M., Laipis, P., Agbandje-McKenna, M., Silverman, D. N., and McKenna, R. (2001) *Biochemistry* **40,** 1741–1748
10. Nair, S. K., and Christianson, D. W. (1991) *J. Am. Chem. Soc.* **113,** 9455–9458
11. Nair, S. K., and Christianson, D. W. (1991) *Biochem. Biophys. Res. Commun.* **181,** 579–584
12. Håkansson, K., Carlsson, M., Svensson, L. A., and Liljas, A. (1992) *J. Mol. Biol.* **227,** 1192–1204
13. Campbell, I. D., Lindskog, S., and White, A. I. (1975) *J. Mol. Biol.* **98,** 597–614
14. Jackman, J. E., Merz, K. M., Jr., and Fierke, C. A. (1996) *Biochemistry* **35,** 16421–16428
15. Scolnick, L. R., and Christianson, D. W. (1996) *Biochemistry* **35,** 16429–16434
16. Krebs, J. F., Fierke, C. A., Alexander, R. S., and Christianson, D. W. (1991) *Biochemistry* **30,** 9153–9160
17. Toba, S., Colombo, G., and Merz, K. M., Jr. (1999) *J. Am. Chem. Soc.* **121,** 2290–2302
18. Lu, D., and Voth, G. A. (1998) *Proteins* **33,** 119–134
19. Lu, D., and Voth, G. A. (1998) *J. Am. Chem. Soc.* **120,** 4006–4014
20. Silhavy, T. J., Berman, M. L., and Enquist, L. W. (1984) *Experiments with Gene Fusions*, Cold Spring Harbor Laboratory Press, Cold Spring Harbor, NY
21. Studier, F. W., Rosenberg, A. H., Dunn, J. J., and Dubendorff, J. W. (1990) *Methods Enzymol.* **185,** 60–89
22. Shiba, K., Ito, K., and Yura, T. (1984) *J. Bacteriol.* **160,** 696–701
23. Miller, J. H. (1972) *Experiments in Molecular Genetics*, Cold Spring Harbor Laboratory Press, Cold Spring Harbor, NY
24. Roth, D. E., Venta, P. J., Tashian, R. E., and Sly, W. S. (1992) *Proc. Natl. Acad. Sci. U. S. A.* **89,** 1804–1808
25. Osborne, W. R., and Tashian, R. E. (1975) *Anal. Biochem.* **64,** 297–303
26. Hunt, J. B., Rhee, M. J., and Storm, C. B. (1977) *Anal. Biochem.* **79,** 614–617
27. Nyman, P., and Lindskog, S. (1964) *Biochim. Biophys. Acta* **85,** 141–151
28. Kakiuchi, K., and Kobayashi, Y. (1971) *J. Biochem.* (*Tokyo*) **69,** 43–52
29. Kishida, K., Miwa, Y., and Iwata, C. (1986) *Exp. Eye Res.* **43,** 981–995
30. Moriyama, H. (1990) *Med. J. Osaka Univ.* **42,** 1–12
31. Bax, A., Ikura, M., Kay, L. E., Torchia, D. A., and Tschudin, R. (1990) *J. Mag. Res.* **86,** 304–318
32. Kay, L. E., Ikura, M., Tschudin, R., and Bax, A. (1990) *J. Mag. Res.* **89,** 496–514
33. Grezesiek, S., and Bax, A. (1992) *J. Mag. Res.* **96,** 432–440
34. Majumdar, A., Wang, H., Morshauser, R., and Zuiderweg, E. R. P. (1993) *J. Biomol. NMR* **3,** 387–397
35. Yamazaki, T., Forman-Kay, J. D., and Kay, L. E. (1993) *J. Am. Chem. Soc.* **115,** 11054–11055
36. Jeener, J., Meier, B. H., Bachmann, P., and Ernst, R. R. (1979) *J. Chem. Phys.* **71,** 4546–4553
37. Gronenborn, A. M., Bax, A., Wingfield, P. T., and Clore, G. M. (1989) *FEBS Lett.* **243,** 93–98
38. Wishart, D. S., Bigam, C. G., and Sykes, B. D. (1995) *J. Biomol. NMR* **6,** 135–140
39. Elguero, J., Marzin, C., Katritzyky, A. R., and Linda, P. (1976) in *Advances in Heterocyclic Chemistry* (Katritzyky, A. R., and Boulton, A. J., eds) pp. 278–281, Academic Press, New York
40. Bachovchin, W. W., and Roberts, J. D. (1978) *J. Am. Chem. Soc.* **100,** 8041–8047
41. Kawano, K., and Kyogoku, Y. (1975) *Chem. Lett.* (*Tokyo*) **1975,** 1305
42. Kyogoku, Y. (1981) *App. Spec. Rev.* **17,** 279–335
43. Bachovchin, W. W. (1986) *Biochemistry* **25,** 7751–7759
44. Shimba, N., Serber, Z., Ledwidge, R., Miller, S. M., Craik, C. S., and Dotsch, V. (2003) *Biochemistry* **42,** 9227–9234
45. Kainosho, M., and Tsuji, T. (1982) *Biochemistry* **21,** 6273–6279
46. Blomberg, F., Maurer, W., and Ruterjans, H. (1977) *J. Am. Chem. Soc.* **99,** 1849–1859
47. Venters, R. A., Farmer, B. T., 2nd, Fierke, C. A., and Spicer, L. D. (1996) *J. Mol. Biol.* **264,** 1101–1116
48. Ozaki, Y., Kyogoku, Y., Ogoshi, H., Sugimoto, H., and Yoshida, Z. (1979) *J. Chem. Soc. Chem. Commun.* **1979,** 76
49. Bao, D., Cheng, J. T., Kettner, C., and Jordan, F. (1998) *J. Am. Chem. Soc.* **120,** 3485–3489
50. Ash, E. L., Sudmeier, J. L., De Fabo, E. C., and Bachovchin, W. W. (1997) *Science* **278,** 1128–1132
51. Roberts, J. D., Yu, C., Flanagan, C., and Birdseye, T. R. (1982) *J. Am. Chem. Soc.* **104,** 3945–3949
52. Schuster, I. I., and Roberts, J. D. (1979) *J. Org. Chem.* **44,** 3864–3867
53. Smedarchina, Z., Siebrand, W., Fernandez-Ramos, A., and Cui, Q. (2003) *J. Am. Chem. Soc.* **125,** 243–251
54. Bottoni, A., Lanza, C. Z., Miscione, G. P., and Spinelli, D. (2004) *J. Am. Chem. Soc.* **126,** 1542–1550
55. Marino, T., Russo, T., and Toscano, M. (2005) *J. Am. Chem. Soc.* **127,** 4252–4253
56. Silverman, D. N. (1995) *Methods Enzymol.* **249,** 479–503
57. Fisher, Z., Hernandez Prada, J. A., Tu, C., Duda, D., Yoshioka, C., An, H., Govindasamy, L., Silverman, D. N., and McKenna, R. (2005) *Biochemistry* **44,** 1097–1105